Front. Phys. China, 2010, 5(2): 166–170
DOI 10.1007/s11467-009-0075-x

RESEARCH ARTICLE

Magnetic excitations of undoped iron oxypnictides

Dao-xin YAO (姚道新)†, E. W. CARLSON

Department of Physics, Purdue University, West Lafayette, IN 47907, USA
E-mail: yaodaoxin@gmail.com

Received August 14, 2009; accepted September 2, 2009

We study the magnetic excitations of undoped iron oxypnictides using a three-dimensional Heisenberg model with single-ion anisotropy. Analytic forms of the spin-wave dispersion, velocities, and structure factor are given. Aside from quantitative comparisons that can be made to inelastic neutron scattering experiments, we also give qualitative criteria that can distinguish various regimens of coupling strength. The magnetization reduction due to quantum zero point fluctuations shows clear dependence on the c-axis coupling.

Keywords iron-based superconductor, 3-D Heisenberg model, spin-wave, neutron scattering, sublattice mangetization

PACS numbers 74.25.Ha, 74.70.-b, 75.30.Ds, 76.50.+g

The discovery of a new class of superconductors with transition temperatures exceeding 55 K has spurred new hope of developing a unified theory of high-temperature superconductivity [1–3]. Like the cuprate superconductors, in the iron pnictide compounds, superconductivity arises from doping a layered antiferromagnet, giving rise to tantalizing similarities in the phase diagrams. However, there are also striking differences. For example, whereas importance is placed on a single d-orbital per Cu site in the cuprates, in the iron-based superconductors importance is placed on several d-orbitals per Fe site, and the total nominal spin per site may be large. Furthermore, the parent compounds of the iron-based materials are semi-metals, rather than Mott insulators as in the cuprate case. In addition, recent experiments have shown that the electronic couplings in the iron-based superconductors are more three-dimensional than in the cuprate superconductors [4–6].

Although static magnetism tends not to survive in the superconducting state of the iron pnictides, magnetic excitations have been shown to play an important role in the superconducting state. In particular, a resonance peak has been associated with superconductivity, suggesting a further connection with cuprate physics. Because of the prominent role of magnetism in these materials and the connection of magnetic fluctuations to the superconducting state, it is important to understand the simpler magnetic excitations that are present in the parent compound. In order to understand the magnetic excitations, we consider an effective Heisenberg model with exchange couplings between the net spin associated with each site. The effective Heisenberg model may be thought to arise from exchange either associated with localized magnetic moments, or associated with the net moment arising from an SDW associated with itinerant electrons.

At room temperature, most undoped iron pnictide superconductors have a tetragonal paramagnetic phase. Upon decreasing temperature, the materials show a structural transition from tetragonal to orthorhombic. In the 122 materials, a three-dimensional long-range antiferromagnetic order develops simultaneously. This phenomenology constrains effective exchange constants in the Heisenberg model, written as [4]:

$$H = J_{1a}\sum_{i,j}\boldsymbol{S}_i\cdot\boldsymbol{S}_j + J_{1b}\sum_{i,j}\boldsymbol{S}_i\cdot\boldsymbol{S}_j + J_2\sum_{i,j}\boldsymbol{S}_i\cdot\boldsymbol{S}_j + J_c\sum_{i,j}\boldsymbol{S}_i\cdot\boldsymbol{S}_j - J_s\sum_i(S_i^z)^2 \quad (1)$$

where J_{1a} and J_{1b} are the nearest neighbor interactions along the a- and b-axes, J_2 is the next nearest neighbor interaction within the plane, J_c is the interaction along c-axis, and J_s is the single-ion anisotropy. These couplings are illustrated in Fig. 1. We use linear spin-wave theory to study the magnetic excitations and sublattice magnetization reduction due to quantum zero-point fluctuations.

We use Holstein–Primakoff bosons to rewrite the above Hamiltonian as [7]:

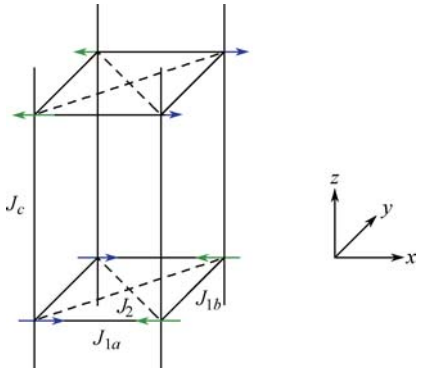

Fig. 1 Typical magnetic structure of undoped iron-based superconductors.

$$H = E_{\rm Cl} + \sum_{\boldsymbol{k}} \left[A_{\boldsymbol{k}} a^\dagger_{\boldsymbol{k}} a_{\boldsymbol{k}} + \frac{1}{2}(B_{\boldsymbol{k}} a^\dagger_{\boldsymbol{k}} a^\dagger_{-\boldsymbol{k}} + B^*_{-\boldsymbol{k}} a_{\boldsymbol{k}} a_{-\boldsymbol{k}}) \right] \tag{2}$$

where $E_{\rm Cl} = (-J_{1a} + J_{1b} - 2J_2 - J_c - J_s)NS^2$ is the classic ground-state energy. The Hamiltonian can be diagonalized by using the Bogoliubov transformation,

$$b_{\boldsymbol{k}} = \cosh(\theta_{\boldsymbol{k}} a_{\boldsymbol{k}}) - \sinh(\theta_{\boldsymbol{k}} a^\dagger_{-\boldsymbol{k}}) \tag{3}$$

which leads to the result

$$H = E_{\rm Cl} + E_o + \sum_{\boldsymbol{k}} \omega(\boldsymbol{k}) b^\dagger_{\boldsymbol{k}} b_{\boldsymbol{k}} \tag{4}$$

where $\omega(\boldsymbol{k})$ is the spin wave dispersion and E_0 is the quantum zero-point energy correction.

The spin wave dispersion $\omega(\boldsymbol{k})$ is given by

$$\omega(\boldsymbol{k}) = \sqrt{A_k^2 - B_k^2} \tag{5}$$

where

$$A_k = 2S(J_{1a} - J_{1b} + 2J_2 + J_s + J_z + J_{1b}\cos k_y) \tag{6}$$

$$B_k = 2S(J_{1a} + 2J_2 \cos k_y)\cos k_x + 2J_c \cos k_z \tag{7}$$

The quantum zero-point energy is then

$$E_0 = \frac{1}{2}\sum_{\boldsymbol{k}} [-A_{\boldsymbol{k}} + \omega(\boldsymbol{k})] \tag{8}$$

The presence or absence of gaps at particular points in the Brillouin zone may be used to gain qualitative information about the state of the system:

$$\begin{aligned}
&\Delta(\pi,0,\pi) = 2S\sqrt{J_s(2J_{1a} + 4J_2 + J_s + 2J_c)} \\
&\Delta(0,\pi,\pi) \\
&\quad = 2S\sqrt{(2J_{1a} - 2J_{1b} + J_s)(-2J_{1b} + 4J_2 + J_s + 2J_c)} \\
&\Delta(\pi,\pi,\pi) \\
&\quad = 2S\sqrt{(-2J_{1b} + 4J_2 + J_s)(2J_{1a} - 2J_{1b} + J_s + 2J_c)} \\
&\Delta(0,0,\pi) = \Delta(\pi,0,\pi)
\end{aligned} \tag{9}$$

For example, there can only be a gap at $\Delta(\pi,0,\pi)$ if single-ion anisotropy is present. Measuring a finite gap at this point requires that J_s be nonzero. In $SrFe_2As_2$, it has been shown that single-ion anisotropy is present, although it is a very weak energy scale, $J_s \approx 0.015$ meV [4]. Given that J_s is a small energy scale, we see that measuring a gap at $\Delta(0,\pi,\pi)$ would indicate that there is anisotropy in the electronic degrees of freedom, i.e. $J_{1a} \neq J_{1b}$. In this sense, the value of $\Delta(0,\pi,\pi)$ may be taken as a measure of electron nematicity in the system. It was furthermore established in Ref. [4] that $J_c \gg J_s$. When this is the case, the magnitude of the gap at $\Delta(\pi,\pi,\pi)$ may be used to indicate proximity to the magnetic phase transition at $J_{1b} = 2J_2$. Because the gaps must be real-valued, we see that the system is constrained to have $J_{1b} \leqslant \min[J_{1a} + \frac{J_s}{2}, 2J_2 + \frac{J_s}{2}]$. Violation of this constraint indicates a change in the ground state.

In the limit of vanishing single-ion anisotropy, the gap at $(\pi,0,\pi)$ disappears, and the following spin-wave velocities can be defined

$$v_x = 2S\sqrt{(J_{1a} + 2J_2)(J_{1a} + 2J_2 + J_c)} \tag{10}$$

$$v_y = 2S\sqrt{(2J_2 - J_{1b})(J_{1a} + 2J_2 + J_c)} \tag{11}$$

$$v_z = 2S\sqrt{J_c(J_{1a} + 2J_2 + J_c)} \tag{12}$$

Notice that v_y becomes imaginary for $J_{1b} > 2J_2$, indicating a change in the classic ground state configuration. This is consistent with the stability condition noted above, which is imposed by requiring that $\Delta(0,\pi,\pi)$ remain real-valued.

First principles calculations of the electronic structure have made two broad categories of predictions: (1) $J_2 > J_{1a} \approx J_{1b}$ [8, 9] and (2) $2J_2 \approx J_{1a} \gg J_{1b}$ [10, 11]. Recent neutron scattering experiments have been used to measure the exchange couplings. However, their results are quite different [5, 12, 13]. Here, we provide further predictions to aid in distinguishing the two cases. Figure 2(a) and (b) show the typical spin-wave spectrum for the two cases. In case (1), there are two small spin-wave gaps at both $(\pi,0,\pi)$ and $(0,\pi,\pi)$. If the system is twinned, two spin gaps may be observed. However, in case (2), the large interaction anisotropy pushes the spin-wave gap at $(0,\pi,\pi)$ up to the high energy, which forms a flat zone boundary for case (2), and only one low-energy spin-wave gap is expected.

The neutron scattering cross-section is proportional to the dynamic structure factor $S(\boldsymbol{k},\omega)$ [5]. In the linear spin-wave approximation, the transverse parts contribute to the structure factor. By symmetry, we have

$$\begin{aligned}
S^{xx}(\boldsymbol{k},\omega) &= S^{yy}(\boldsymbol{k},\omega) \\
&= g^2\mu_{\rm B}^2 S_{\rm eff} \frac{A_k - B_k}{2\omega(\boldsymbol{k})}[n(\omega)+1]\Delta(\omega - \omega(\boldsymbol{k}))
\end{aligned} \tag{13}$$

where $S_{\rm eff}$ is the effective spin on an Fe ion, g is the g-factor of iron (~ 2), and $n(\omega)$ is the Bose occupation factor.

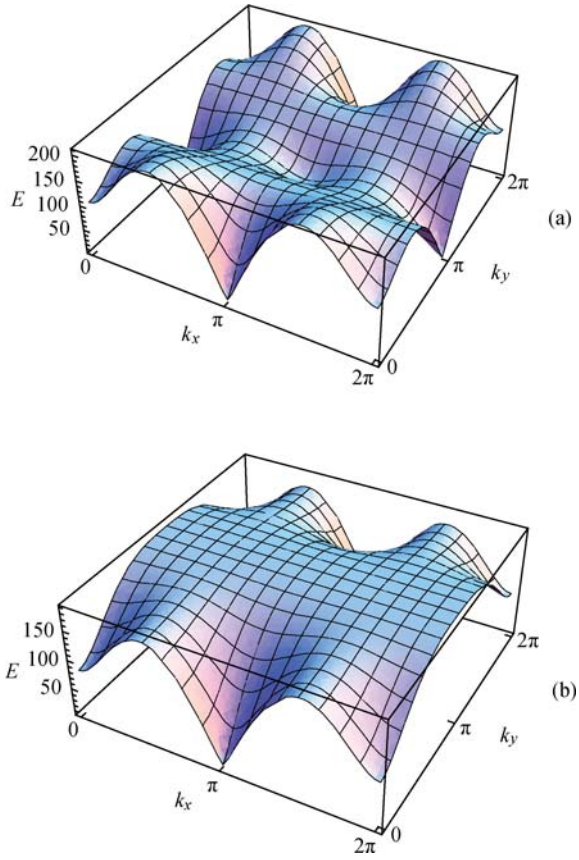

Fig. 2 Spin-wave dispersion band for the antiferromagnet shown in Fig. 1. **(a)** Dispersion for $J_{1a} = J_{1b}$, which corresponds to $J_{1a} = 25$, $J_{1b} = 25$, $J_2 = 36$, $J_c = 7$, and $J_S = 0.05$. **(b)** Dispersion with $J_{1a} \gg J_{1b}$, which corresponds to $J_{1a} = 40$, $J_{1b} = -5$, $J_2 = 20$, $J_c = 5$, and $J_S = 0.05$.

In Fig. 3, we show intensity plots at constant energy for the dynamic structure factor $S(\boldsymbol{k}, \omega)$, assuming a crystal with twinned antiferromagnetic domains. In the presence of twinning, two concentric spin wave rings are expected at low energy if the neutron scattering resolution is high enough for case (1). At high energy, the outer ring increases quicky for case (1) and can form bright spots as the rings merge. In case (2), only one ring will be observed since the energy gap at $(0, \pi, \pi)$ goes to very high energy. In addition, the band top in case (2) becomes flat in a very large portion of the Brillouin zone. [See Fig. 2(b)].

The integrated structure factor $S(\omega)$ can also be used to distinguish the two cases:

$$S(\omega)^{\alpha\alpha} = \iiint_{\mathrm{BZ}} \mathrm{d}k_x \mathrm{d}k_y \mathrm{d}k_z S^{\alpha\alpha}(\boldsymbol{k}, \omega) \Delta(\omega - \omega(\boldsymbol{k})) \tag{14}$$

where $\alpha = x, y$ and BZ means integrate over the full magnetic Brillouin zone. Numerical results are presented in Fig. 4. The most dramatic differences are expected in the high-energy response. There are two broad peaks expected for the $J_{1a} = J_{1b}$ case. There is a sharp peak at high energy for the $J_{1a} \gg J_{1b}$ case, which is caused by

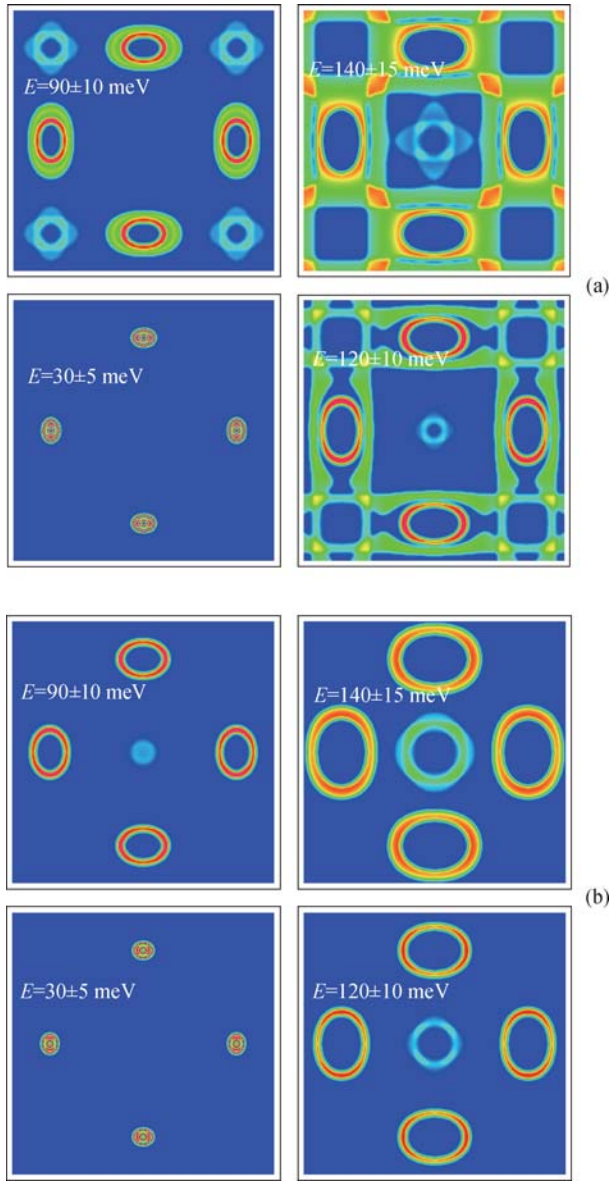

Fig. 3 Constant-energy cuts (twinned) of the dynamic structure factor $S(\boldsymbol{k}, \omega)$ for **(a)** $J_{1a} = J_{1b}$ and **(b)** $J_{1a} \gg J_{1b}$. The x-axis and y-axis correspond to k_x and k_y respectively, with the range $(-1.5\pi, 1.5\pi)$. Interaction parameters are same as Fig. 2.

the very large density of states near the spin-wave zone boundary. As we see from Fig. 2(b), the spin-wave band is flat in a large portion of the Brillouin zone. We also show a curve of $S(\omega)$ for the case of $J_{1a} = 2J_{1b}$ (J_{1a} is not much bigger than J_{1b}).

The total moment sum rule for a Heisenberg model with spin S is defined as [14]:

$$\begin{aligned} M_0 &= \frac{1}{N} \sum_{\alpha} \int \mathrm{d}\boldsymbol{k} \int_{-\infty}^{\infty} \mathrm{d}\omega S^{\alpha\alpha}(\boldsymbol{k}, \omega) \\ &= M^x + M^y + M^z \\ &= g^2 \mu_{\mathrm{B}}^2 S(S+1) \end{aligned} \tag{15}$$

The transverse part of this corresponds to $M^{\alpha} = \frac{1}{N} \int \int \int_{\mathrm{BZ}} \mathrm{d}k_x \mathrm{d}k_y \mathrm{d}k_z \int \mathrm{d}\omega S^{\alpha\alpha}(\boldsymbol{k}, \omega)$, where $\alpha = x, y$.

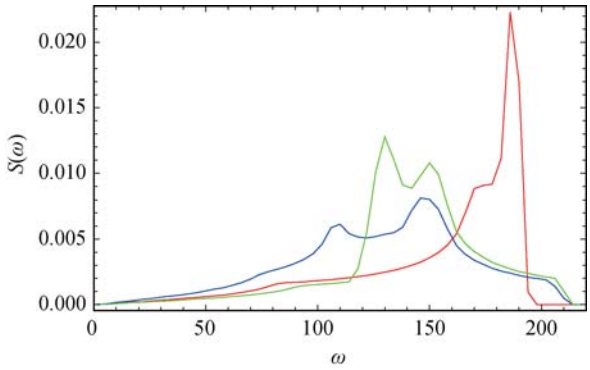

Fig. 4 $S(\omega)$ for the full Brillouin zone. The blue line corresponds to case (1) $J_{1a} = J_{1b}$, the red line corresponds to $J_{1a} \gg J_{1b}$, and the green line is for an intermediate case that has $J_{1a} = 40$, $J_{1b} = 20$, $J_2 = 30$, $J_c = 5$, $J_s = 0.05$. Interaction parameters in cases (1) and (2) are same as Fig. 2. $S(\omega)$ is in units of $g^2\mu_B^2 S_{\text{eff}}$.

We get $M^x = M^y = 0.61 g^2 \mu_B^2 S_{\text{eff}}$ per Fe for case (1) and $M^x = M^y = 0.58 g^2 \mu_B^2 S_{\text{eff}}$ per Fe for case (2).

The measured magnetic moment per iron is typically less than one Bohr magneton (μ_B), which is much smaller than the theoretically expected value of $\sim 2.3\mu_B$ per iron site predicted by LDA calculations [8, 15, 16]. In spin-wave theory, both the quantum zero-point fluctuations and thermal fluctuations reduce the expected magnetic moment per site. Since the energy scale of iron-based superconductors is much larger than the temperature scale, we focus on the the quantum zero-point fluctuations. The sublattice magnetization reduction $\Delta m^{\text{quantum}}$ is defined as:

$$\Delta m^{\text{quantum}} = \frac{1}{2}\int_0^{2\pi}\int_0^{2\pi}\int_0^{2\pi}\frac{\mathrm{d}k_x}{2\pi}\frac{\mathrm{d}k_y}{2\pi}\frac{\mathrm{d}k_z}{2\pi}\frac{A_{\boldsymbol{k}}}{\omega(\boldsymbol{k})} - \frac{1}{2} \tag{16}$$

In Fig. 5, we present the numerical results for both cases (1) and (2). Note that J_c has an important effect on the magnetization reduction. Empirically, the 122 materials are generally more three-dimensional than the 1111 materials [17]. Thus, the effective magnetic moment for 122 material is expected to be higher than 1111 materials. If $J_c \approx 5$ meV, we have $\Delta m^{\text{quantum}} \approx 0.1$. For $S = 1/2$, this gives $S_{\text{eff}} \approx 0.4$, which is close to the magnetic moment found by experiments in the 122 materials, which have $gS_{\text{eff}} \approx 0.8\mu_B$ [17].

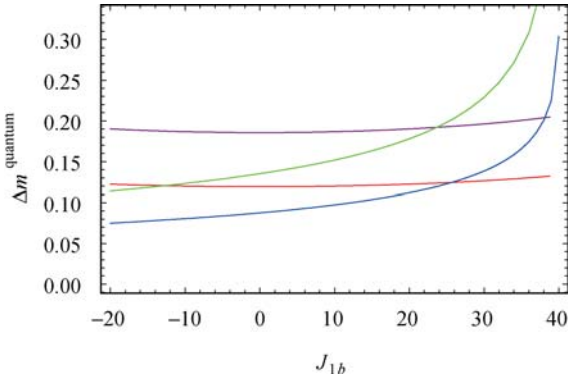

Fig. 5 J_{1b}/J_{1a} dependence of the reduction of the sublattice magnetization due to zero point energy of the spin-waves. Red ($J_c = 5$ meV) and purple ($J_c = 0$ meV) lines correspond to $J_{1a} = J_{1b}$, blue ($J_c = 5$ meV) and green ($J_c = 0$) lines correspond to $J_{1a} \gg J_{1b}$. Interaction parameters are same as Fig. 2.

In summary, we have used the three-dimensional Heisenberg model and spin-wave theory to study the magnetic excitations, dynamic structure factor, and sublattice magnetization for the antiferromagnetic spin state found in the undoped iron-based superconductors. The anisotropy of exchange couplings within the Fe–As plane can cause clear differences in the spin-wave spectrum, expected scattering intensity at constant energy, and integrated dynamic structure factor. These can be used to determine the degree of anisotropy of magnetic exchange interactions within the Fe–As plane. To fully understand the anisotropy, one may need to consider both the localized electrons and itinerant electrons in the undoped iron-based superconductors [13, 18]. In addition, we have calculated the sublattice magnetization reduction from the quantum zero-point fluctuation. The results show that J_c can enhance the long-range magnetic ordering dramatically, which is consistent with the experimental findings about the magnetic moments in 1111 and 122 materials.

Acknowledgements We thank J. P. Hu, P. Dai, J. Zhao, S. Li and E. Dagotto for helpful discussions. This work was supported by Research Corporation and by NSF Grant No. DMR 08-04748.

References

1. Y. Kamihara, T. Watanabe, M. Hirano, and H. Hosono, J. Am. Chem. Soc., 2008, 130: 3296
2. Z. A. Ren, W. Lu, J. Yang, W. Yi, X. L. Shen, Z. C. Li, G. C. Che, X. L. Dong, L. L. Sun, F. Zhou, and Z. X. Zhao, Chin. Phys. Lett., 2008, 25: 2215
3. C. Wang, L. Li, S. Chi, Z. Zhu, Z. Ren, Y. Li, Y. Wang, X. Lin, Y. Luo, S. Jiang, X. Xu, G. Cao, and Z. Xu, Europhys. Lett., 2008, 83: 67006
4. J. Zhao, D. X. Yao, S. Li, T. Hong, Y. Chen, S. Chang, W. R. II, J. W. Lynn, H. A. Mook, G. F. Chen, J. L. Luo, N. L. Wang, E. W. Carlson, J. P. Hu, and P. Dai, Phys. Rev. Lett., 2008, 101: 167203
5. R. Ewings, T. Perring, R. Bewley, T. Guidi, M. Pitcher, D. R. Parker, S. J. Clarke, and A. T. Boothroyd, Phys. Rev. B, 2008, 78: 220501(R)
6. H. Q. Yuan, J. Singleton, F. F. Balakirev, S. A. Baily, G. F. Chen, J. L. Luo, and N. L. Wang, Nature, 2009, 457: 565
7. D. X. Yao and E. W. Carlson, Phys. Rev. B, 2008, 78: 052507
8. F. Ma and Z. Y. Lu, Phys. Rev. B, 2008, 78: 033111
9. T. Yildirim, Phys. Rev. Lett., 2008, 101: 057010
10. Z. P. Yin, S. Lebègue, M. J. Han, B. P. Neal, S. Y. Savrasov, and W. E. Pickett, Phys. Rev. Lett., 2008, 101: 047001
11. M. J. Han, Q. Yin, W. E. Pickett, and S. Y. Savrasov, Phys. Rev. Lett., 2009, 102: 107003

12. S. O. Diallo, V. P. Antropov, C. Broholm, T. G. Perring, J. J. Pulikkotil, N. Ni, S. L. Budko, P. C. Canfield, A. Kreyssig, A. I. Goldman, and R. J. McQueeney, Phys. Rev. Lett., 2009, 102: 187206
13. J. Zhao, D. T. Adroja, D. X. Yao, R. Bewley, S. Li, X. F. Wang, G. Wu, X. H. Chen, J. P. Hu, and P. Dai, Nature Physics, 2009, 5: 555
14. J. Lorenzana, G. Seibold, and R. Coldea, Phys. Rev. B, 2005, 72: 224511
15. C. Cao, P. J. Hirschfeld, and H. P. Cheng, Phys. Rev. B, 2008, 77: 220506(R)
16. J. Dong, H. J. Zhang, G. Xu, Z. Li, G. Li, W. Z. Hu, D. Wu, G. F. Chen, X. Dai, J. L. Luo, Z. Fang, and N. L. Wang, Europhys. Lett., 2008, 83: 27006
17. J. W. Lynn and P. Dai, Physica C, 2009, 469: 469
18. P. M. R. Brydon and C. Timm, arxiv: 0909.1222, 2009